Neurobiology of Disease 206 (2025) 106826

Contents lists available at ScienceDirect

Neurobiology of Disease

journal homepage: www.elsevier.com/locate/ynbdi

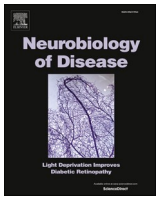

CRISPR-based epigenetic editing of *Gad1* improves synaptic inhibition and cognitive behavior in a Tauopathy mouse model

Lei Wan, Ping Zhong, Pei Li, Yong Ren, Wei Wang, Mingjun Yu, Henry Y. Feng, Zhen Yan *

Department of Physiology and Biophysics, Jacobs School of Medicine and Biomedical Sciences, State University of New York at Buffalo, Buffalo, NY 14214, USA

ARTICLE INFO

Keywords:
Alzheimer's disease
GABAergic transmission
GAD1
Histone acetylation
CRISPR
Prefrontal cortex
Spatial memory

ABSTRACT

GABAergic signaling in the brain plays a key role in regulating synaptic transmission, neuronal excitability, and cognitive processes. Large-scale sequencing has revealed the diminished expression of GABA-related genes in Alzheimer's disease (AD), however, it is largely unclear about the epigenetic mechanisms that dysregulate the transcription of these genes in AD. We confirmed that GABA synthesizing enzymes, *GAD1* and *GAD2*, were significantly downregulated in prefrontal cortex (PFC) of AD human postmortem tissues. A tauopathy mouse model also had the significantly reduced expression of GABA-related genes, as well as the diminished GABAergic synaptic transmission in PFC pyramidal neurons. To elevate endogenous Gad1 levels, we used the CRISPR/Cas9-based epigenome editing technology to recruit histone acetyltransferase p300 to *Gad1*. Cells transfected with a fusion protein consisting of the nuclease-null dCas9 protein and the catalytic core of p300 ($dCas9^{p300}$), as well as a guide RNA targeting *Gad1* promoter ($gRNA^{Gad1}$), had significantly increased *Gad1* mRNA expression and histone acetylation at *Gad1* promoter. Furthermore, the tauopathy mouse model with PFC injection of $dCas9^{p300}$ and $gRNA^{Gad1}$ lentiviruses had significantly elevated GABAergic synaptic currents and improved spatial memory. These results have provided an epigenetic editing-based gene-targeting strategy to restore synaptic inhibition and cognitive function in AD and related disorders.

1. Introduction

Alzheimer's disease (AD), a leading cause of dementia, is manifested as the impaired memory, speech, visuospatial processing and executive functions (Knopman et al., 2021; Long and Holtzman, 2019). While pathological hallmarks, β-amyloid (Aβ)-containing extracellular plaques and tau-containing intracellular neurofibrillary tangles, have been found in AD (Wilson 3rd et al., 2023), the effective treatment for cognitive deficits of AD is still limited (De Strooper and Karran, 2016; Wilson 3rd et al., 2023).

In cognitive regions like neocortex, the balanced excitatory and inhibitory synaptic activity plays a fundamental role in neuronal computation (Froemke, 2015; Okur et al., 2024). A variety of neurodegenerative diseases have excitation/inhibition (E/I) imbalance, including frontotemporal lobar degeneration (Huber et al., 2022), amyotrophic lateral sclerosis (Kiernan et al., 2011; Pasinelli and Brown, 2006), Huntington disease (Li et al., 2003), multiple sclerosis (Mandolesi et al., 2015) and AD (Ghatak et al., 2021; Harris et al., 2020; Palop and Mucke, 2016; Wilson 3rd et al., 2023). The increased E/I ratio in parietal cortex has been reported in middle-aged AD patients of early onset (Lauterborn et al., 2021). Seizures, which indicate neuronal hyperexcitability and network synchrony, can emerge several years preceding the cognitive problems and may persist into the dementia stage of AD patients (Harris et al., 2020). The incidence of seizure is 7–8 times higher in individuals with AD than in people without dementia (Palop and Mucke, 2016), and seizures can hasten the cognitive decline in AD patients (Vossel et al., 2017). AD mouse models expressing mutated human Aβ precursor protein (hAPP) (Verret et al., 2012) or tau (A152T) (Maeda et al., 2016) also have epileptic activity.

Although E/I imbalance occurs in both prodromal AD patients and AD animal models, the underlying mechanism remains elusive. A systemic review with meta-analysis has shown GABA deficits in AD human brains, including the lower GABA levels and the downregulation of GAD65/67, $GABA_A$ receptors, and GABA transporters (Carello-Collar et al., 2023). Inhibitory neurons are also found to be correlated with cognitive resilience in late life of AD (Mathys et al., 2023). Here we demonstrated the loss of GABA-related molecules, such as GABA synthesizing enzyme *Gad1*, in AD, which was correlated with the

* Corresponding author at: State University of New York at Buffalo, 955 Main St., Buffalo, NY, USA.
E-mail address: zhenyan@buffalo.edu (Z. Yan).

https://doi.org/10.1016/j.nbd.2025.106826
Received 8 October 2024; Received in revised form 30 January 2025; Accepted 30 January 2025
Available online 1 February 2025

diminished GABAergic transmission in prefrontal cortical pyramidal neurons.

Emerging evidence indicates that CRISPR-based epigenome editing provides a powerful approach to reorganize chromatin architecture and alter endogenous gene expression at specific loci (Goell and Hilton, 2021; Nakamura et al., 2021; Pulecio et al., 2017; Thakore et al., 2016). One of the strategies is to recruit histone acetyltransferase p300 to the promoters or enhancers of specific genes to enable their upregulation via increased histone acetylation (Hilton et al., 2015). In this study, we used this CRISPR-based epigenetic editing technology to elevate endogenous *Gad1*, and revealed the therapeutic potential of this gene-targeting approach on synaptic and behavioral deficits in a tauopathy mouse model.

2. Results

2.1. Bioinformatic analysis and mRNA profiling reveal the loss of GABA-related genes in postmortem brains of AD patients

From a microarray dataset (Zhang et al., 2013), we have identified many downregulated differentially expressed genes (Down DEGs) in frontal cortex of AD samples (Williams et al., 2021). Using SynGo, a synaptic gene ontology database, we found that these Down DEGs were synaptic enriched, particularly in synaptic organization, postsynaptic and presynaptic signaling (Fig. 1A**, Sup. Table 1**). Using Gene Ontology (GO) analysis of two RNAseq databases from Mayo Clinic and Mount Sinai (Allen et al., 2016; Wang et al., 2018), we found that the common Down DEGs in AD were enriched in trans-synaptic signaling, GABAergic and glutamatergic synaptic transmission and neurotransmitter release (Fig. 1B**, Sup. Table 2**). Protein-protein interaction (PPI) networks (Fig. 1C) showed the strong connections of these downregulated synaptic genes, which could be clustered into 3 groups: GABA-related genes, including those encoding GABA synthesis enzymes (*GAD1* and *GAD2*), $GABA_A$ receptors (*GABRA1/2*, *GABRB2* and *GABRG2*), vesicular GABA transporter (*SLC32A1*) and potassium-chloride co-transporter (*SLC12A5*); glutamate-related genes, including those encoding ionotropic and metabotropic glutamate receptors (*GRIA1/3*, *GRIN2A/2B* and *GRMs*) and vesicular glutamate transporters (*SLC17A6/7*); and genes related to synaptic organization and transmitter release (*NRXN1, SNAP25*, *SYNs*, *SYTs*). These data have confirmed the loss of synaptic genes in AD, which may play a key role in synaptic dysfunction in this disease condition (Brose et al., 2010; Mucke and Selkoe, 2012; Selkoe, 2002).

The loss of GABA-related genes has been implicated in AD pathology (Carello-Collar et al., 2023; Mathys et al., 2023), so we examined the trajectory of their changes in AD. Using the scRNA-seq SEA-AD dataset (Gabitto et al., 2024), we found that the expression of many GABA-related genes exhibited the profound reduction in a cell type-specific manner during AD pseudo-progression (Fig. 1D), including *GAD1*, *GAD2* and three markers of GABAergic neuron subtypes: parvalbumin (*PVALB*), somatostatin (*SST*) and vasoactive intestinal peptide (*VIP*), while the $GABA_A$ receptor gene, *GABRG2*, was largely unchanged across various cell types. We then used quantitative PCR (qPCR) to verify the changes of GABA-related genes with our AD human postmortem prefrontal cortical tissue. Compared with normal controls, the expression *GAD1*, *GAD2*, *SST* and *VIP* was significantly reduced in AD samples, and some $GABA_A$ receptor genes (*GABRA1* and *GABRG2*) showed the trend of reduction (Fig. 1E), confirming the strong loss of GABA-related genes in AD humans.

To find out whether the altered inhibition-related transcripts are also reduced at the protein level, we performed Western blotting experiments to compare GAD67 (encoded by *GAD1*) protein levels in control vs. AD human postmortem PFC. As shown in Fig. 1F, AD samples exhibited a significantly lower level of GAD67 protein expression, compared to controls, further suggesting that GABA synthesis is diminished in AD.

2.2. GABA-related gene expression and GABAergic synaptic transmission are compromised in the PFC of a tauopathy mouse model

Next, we sought to determine whether GABA-related genes were also altered in AD-related mouse models. To this end, we analyzed the RNA-seq data in sorted neurons from WT and P301S Tau mice (GSE129797) (Wu et al., 2019). GO analysis indicated that the top Down DEGs in Tau mice were enriched in GABAergic synaptic transmission, GABA signaling, inhibitory synapse assembly and chloride transmembrane transport (Fig. 2A**, Sup. Table 3**). PPI of Down DEGs in the top GO categories included the strongly connected $GABA_A$ receptors (Gabra1/4, Gabrb2/3, Gabrg2) (Fig. 2B).

We performed qPCR to verify the downregulation of GABA-related genes in Tau mice. We found that (Fig. 2C & 2D) genes encoding GABA synthesizing enzymes (Gad1/2), GABA transporters (*Slc6a1* and *Slc32a1*), GABA receptor (*Gabrg2*) and neurotransmitter release (*Stx1a*) were significantly decreased in PFC of Tau mice, while other genes (*Sst, Vip, Gabrb2/a2/a1, Tubb2a*) were unchanged.

To find out whether the loss of GABA-related gene expression in Tau mice may lead to diminished inhibitory synaptic transmission, we performed patch-clamp recordings of PFC pyramidal neurons. As shown in Fig. 3A and B, $GABA_A$ receptor-mediated inhibitory postsynaptic currents ($GABA_A$R-IPSC) evoked by a range of stimulation intensities were significantly smaller in Tau mice. The paired-pulse ratio (PPR) of $GABA_A$R-IPSC, a measure of presynaptic release probability, was significantly different between WT and Tau mice (Fig. 3C). The frequency, but not amplitude, of spontaneous IPSC (sIPSC) was also significantly reduced in Tau mice (Fig. 3D and E), suggesting that changes in presynaptic GABA release could contribute to the reduced GABAergic synaptic response.

2.3. CRISPR/Cas9-based epigenome editing boosts the expression of Gad1

With the deficiency of GABAergic transmission in PFC of Tau mice, we next examined the therapeutic avenue to restore synaptic inhibition. Since genes related to GABA synthesis, GABA release, GABA transport and GABA receptors were downregulated in AD, we decided to boost the expression of GABA synthesis enzyme *Gad1* using CRISPR activation (CRISPRa), a technique to activate gene expression endogenously (Hilton et al., 2015; Li et al., 2020). The system (Fig. 4A) contains two components (Hilton et al., 2015, Li et al., 2020): one is deactivated *S. pyogenes* Cas9 (dCas9 with mutations of D10A and H840A) fused with the core domain of histone acetyltransferase p300 ($dCas9^{p300}$); and the other is a single guide RNA (sgRNA) with 20 bp guide sequence specifically designed to target the protomer region (~200 bp upstream the transcription start site) of *Gad1* ($gRNA^{Gad1}$). After transfection of the two components into N2a cells, we found that the expression of *Gad1* was significantly elevated, while neither $dCas9^{p300}$ nor $gRNA^{Gad1}$ alone could affect *Gad1* expression (Fig. 4B). In addition, the expression of three genes with similar promoter sequences as *Gad1* (*Dgat1, Kcnip3, Lrp2*) was unchanged by dual transfection of $dCas9^{p300}$ and $gRNA^{Gad1}$ (Fig. 4B), suggesting that off-target effect is not a significant issue with this approach.

To find out whether the increased expression of *Gad1* is due to increased histone acetylation, we performed chromatin immunoprecipitation combined with quantitative PCR (ChIP-qPCR) assays using primers at *Gad1* promoter region with enriched histone 3 lysine 9 acetylation (H3K9ac) (Fig. 4C). We found a significant increase of H3K9ac occupancy at *Gad1* promoter in N2a cells transfected with $dCas9^{p300}$ & $gRNA^{Gad1}$, compared to those cells transfected with $gRNA^{Gad1}$ control (Fig. 4D). These data indicate that *Gad1* expression can be elevated by the CRISPR-based epigenetic editing technique.

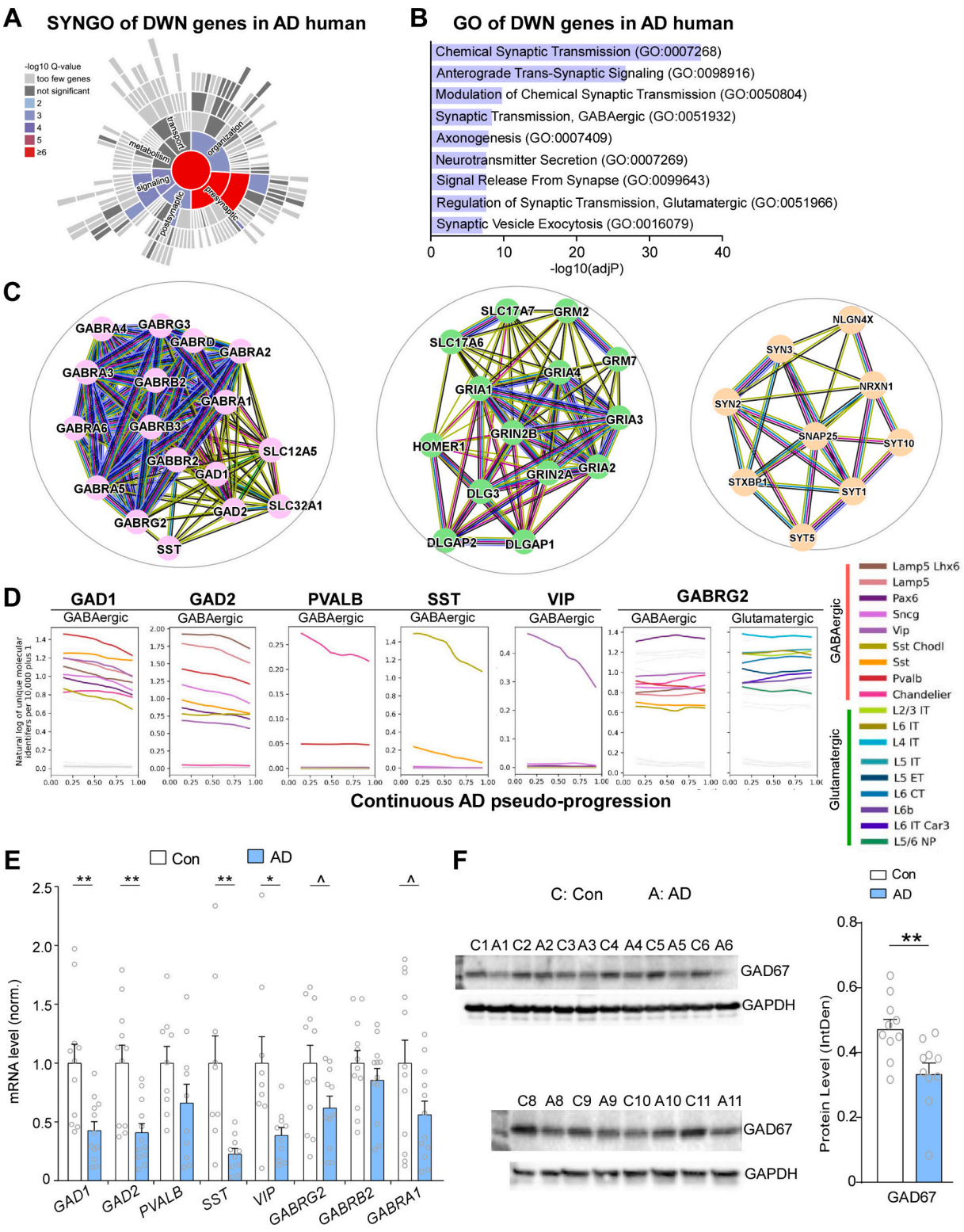

Fig. 1. GABA-related genes are downregulated in AD humans. **A**, Sunburst plot from Synaptic Gene Ontologies (SYNGO) analysis illustrating the downregulated (DWN) genes in AD humans from a microarray dataset. **B**, Gene Ontologies (GO) showing the enriched pathways of common DWN genes in AD humans from two RNAseq datasets (Mayo and MSBB). **C**, Protein-protein interaction (PPI) networks of downregulated genes in AD (pink: GABAergic inhibitory synapse genes; green: glutamatergic excitatory synapse genes; orange: presynaptic genes). **D**, GABA-related gene expression changes across AD pseudo-progression in different cell types. **E**, Bar graphs showing the mRNA level of GABA-related genes in control vs. AD human postmortem brain tissue (control: $n = 9$–12, AD: $n = 11$–12, $P = 0.003$ (*GAD1*); $P = 0.002$ (*GAD2*); $P = 0.003$ (SST); $P = 0.014$ (VIP), $P = 0.05$ (GABRG2); $P = 0.07$ (GABRA1); unpaired *t*-test). **F,** Bar graphs showing GAD67 protein levels in control vs. AD human postmortem brain tissue (control: $n = 10$, AD: n = 10, $P = 0.0073$, unpaired t-test). Insets: Representative Western blots of GAD67. GAPDH was used as a loading control. Data (E, F) are shown as mean ± SEM. $^{\wedge}P < 0.1$, $^{*}P < 0.05$, $^{**}P < 0.01$. (For interpretation of the references to colour in this figure legend, the reader is referred to the web version of this article.)

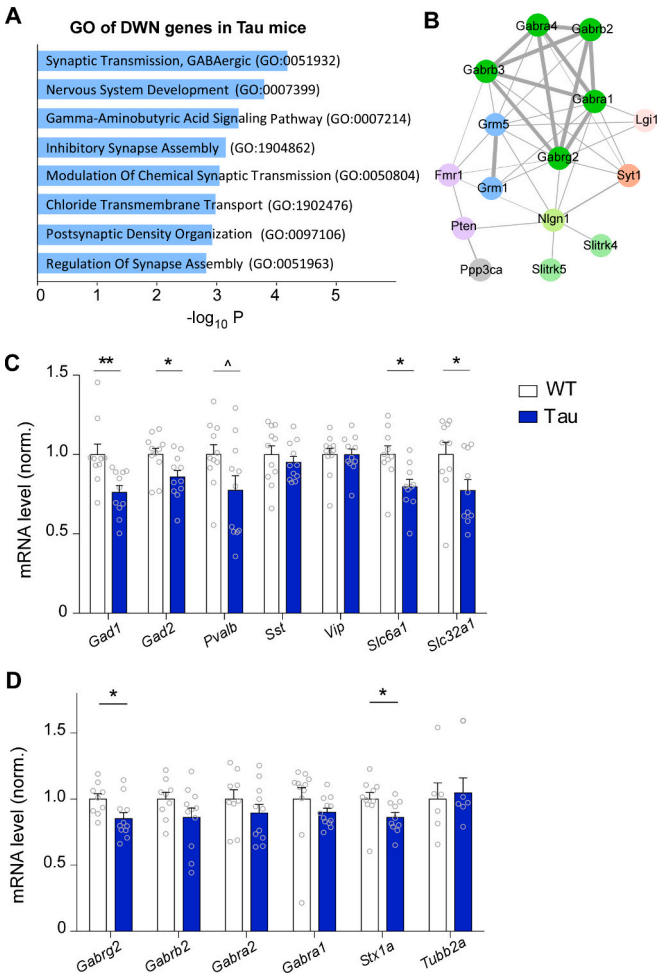

Fig. 2. GABA-related genes are downregulated in Tau mice. **A**, GO showing the enriched pathways of downregulated genes in Tau mice. **B**, PPI network of the downregulated genes in top GO category (GABAergic synaptic transmission) from A. **C,D**, Bar graphs showing the mRNA level of GABA-related genes in wild type (WT) and Tau mice (control: $n = 6$–11, AD: n = 6–12, $P = 0.006$ (*Gad1*); $P = 0.023$ (*Gad2*); $P = 0.01$ (*Slc6a1*); $P = 0.042$ (*Slc32a1*); $P = 0.028$ (*Gabrg2*); $P = 0.043$ (*Stx1a*); unpaired t-test). Data (C & D) are shown as mean ± SEM. ^P < 0.1, *P < 0.05, **P < 0.01.

2.4. CRISPR-based epigenetic editing of Gad1 restores GABAergic transmission and improves spatial memory in Tau mice

Next, we examined the consequences of CRISPR-based epigenetic editing of *Gad1* in vivo by injecting both dCas9^{p300} and gRNA^{Gad1} (GFP-tagged) lentiviruses bilaterally into mouse medial PFC. The viral expression was observed throughout cingulate cortex, prelimbic and infralimbic cortex (Fig. 5A). The significantly increased level of *Gad1* expression in GFP-positive PFC dissected from the dual virus-injected mice (Fig. 5B) indicated the validity of this approach. Patch-clamp recordings indicated that Tau mice with the PFC-injection of dCas9^{p300} & gRNA^{Gad1} lentiviruses had significantly elevated $GABA_A$R-IPSC, compared to Tau mice injected with gRNA^{Gad1} alone (Fig. 5C). It suggests that the diminished GABAergic transmission in Tau mice can be restored by boosting the expression of endogenous *Gad1*.

We further examined the behavioral effect of CRISPR-based epigenetic editing of *Gad1* in Tau mice. Our previous studies have revealed the spatial memory deficits of Tau mice in Barnes maze (BM) tests (Cao et al., 2023; Cao et al., 2020; Wang et al., 2021; Williams et al., 2023). Consistently, in Tau mice (3–4 months old), we found the significantly decreased spatial memory index, which was calculated as the ratio of time spent on the correct hole (T1) and the time on all incorrect holes (T2) in BM tests (Fig. 6A). About ~1 month after bilateral injection of dual lentiviruses (dCas9^{p300} and gRNA^{Gad1}) into mPFC of Tau mice, the spatial memory index was significantly improved, while Tau mice injected with gRNA^{Gad1} lentivirus alone still had poor performance indicated by the low index (Fig. 6B and C). Comparing the individuals of pre- and post-injection testing results, we also found the significantly higher spatial memory index in Tau mice with PFC injection of dual lentiviruses (dCas9^{p300} and gRNA^{Gad1}), but not gRNA^{Gad1} lentivirus alone (Fig. 6D). Together, the data suggest that behavioral deficits of Tau mice can be mitigated by elevating *Gad1* expression.

3. Discussion

3.1. Alterations of GABA-related genes in AD

In the study, we identified the significantly decreased expression of GABA-related genes in AD humans, including genes encoding GABA synthesizing enzymes (*GAD1* and *GAD2*), marker genes of GABAergic neuronal subtypes (*SST* and *VIP*), and some $GABA_A$ receptor genes (*GABRG2* and *GABRA1*). These results are congruent with previous microarray and RNAseq studies of AD humans (Allen et al., 2016; Govindpani et al., 2020; Wang et al., 2018; Zhang et al., 2013). In a meta-analysis of many microarray datasets, both *GAD1* and *GAD2* were found to be significantly reduced in multiple regions of AD humans (Hill and Gammie, 2022). Single-cell RNAseq data also found the decreased GABA-related genes in AD human PFC (Gabitto et al., 2024; Mathys et al., 2023). These results support the hypothesis that the hyperactivity of neural network resulting from the loss of GABAergic inhibition (Carello-Collar et al., 2023) may occur at the early stage of AD, contributing to the progression of the disease through excitotoxicity and seizure episodes (Ghatak et al., 2021; Harris et al., 2020; Kazim et al., 2021; Palop and Mucke, 2016; Vossel et al., 2017).

3.2. Functional implications of GABA-related gene alterations in AD

Mice expressing the human mutant *tau* gene (P301S) have detectable synaptic loss and cognitive deficits at 3 months of age (Cao et al., 2023), followed by tau tangle at 6 months of age in hippocampus and cortex (Yoshiyama et al., 2007; Zhong et al., 2024). We found the significantly reduced GABA-related genes in PFC of Tau mice, including *Gad1/2, Slc6a1* (encoding Gat1), *Slc32a1* (encoding Vgat) and *Gabrg2*. Similarly, in an AD mouse model with both Aβ plaque and Tau tangle pathologies, $GABA_A$ receptor subunits (*Gabrg3/Gabrr1/Gabrr2*) were significantly downregulated (Mori et al., 2023).

Our electrophysiological studies found the diminished inhibitory transmission in PFC pyramidal neurons of Tau mice. Consistently, electroencephalography (EEG) study indicated that young but not old mice expressing P301S Tau had hyperactive network (Van Erum et al., 2020). Network hyperexcitability was also detected in other tauopathy models (Garcia-Cabrero et al., 2013; Maeda et al., 2016). By contrast, in vivo two-photon calcium imaging revealed the reduced activity of neuronal circuits in frontal cortex of P301S tau mice (Marinkovic et al., 2019). The discrepancy could be due to different methods used in activity measurements. Nevertheless, since synaptic inhibition is just one of the factors affecting neural activity, and glutamatergic transmission is also diminished in PFC pyramidal neurons of Tau mice (Cao et al., 2020; Wang et al., 2021; Williams et al., 2023), the final net outcome on neuronal activity is determined by the integration of all intrinsic and synaptic changes.

3.3. Viability of epigenetic editing as a treatment option for AD

Epigenetic editing has emerged as a specific and durable technique to manipulate gene expression without changing the genomic DNA sequences for the treatment of human diseases (Cappelluti et al., 2024; Liu

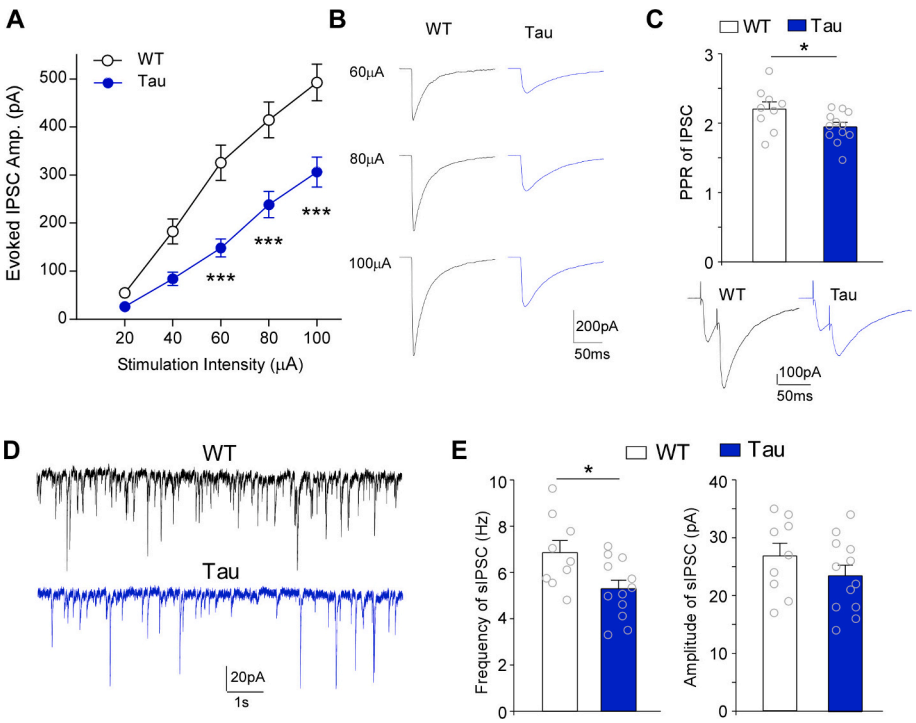

Fig. 3. GABAergic synaptic transmission is diminished in Tau mice. **A**, Input-output curves of evoked $GABA_AR$-IPSC in PFC pyramidal neurons from WT vs. Tau mice (WT: $n = 29$ cells/3 mice; Tau: $n = 19$ cells/3 mice, two-way rmANOVA). **B**, Representative $GABA_AR$-IPSC traces at various stimulation intensities. **C**, Plot of paired-pulse ratio (PPR) of GABAAR-IPSC evoked by double pulses at 25-ms interval in PFC pyramidal neurons from WT vs. Tau mice (WT: n = 9 cells/2 mice; Tau: $n = 12$ cells/3 mice, $P = 0.037$, unpaired t-test). **D, E,** Representative sIPSC traces and bar graphs of sIPSC amplitudes and frequencies in PFC pyramidal neurons from WT vs. Tau mice (WT: n = 9 cells/2 mice; Tau: n = 12 cells/3 mice, amp: $P = 0.26$, freq: $P = 0.02$, unpaired t-test). All data are shown as mean ± SEM. *P < 0.05, ***$P < 0.001$.

and Jaenisch, 2019; Neumann et al., 2024). By fusing an engineered zinc finger domain that binds to Dlg4/PSD95 promoter with histone methyltransferase G9a, an artificial epigenetic editor (methylating H3K9) was generated to achieve the specific repression of Dlg4/PSD95, which demonstrated the significance of Dlg4/PSD95 in aging and AD (Bustos et al., 2017). The CRISPR-based approach can achieve the simple targeting of different genomic DNAs by altering the guide sequence within sgRNA, therefore enabling researchers to site-specifically program epigenetic modifications to DNA and histones, resulting in the dynamic alteration of chromatin architecture and gene transcription at specific loci (Pulecio et al., 2017; Thakore et al., 2016).

A CRISPR/Cas9-based technique using the nuclease-null dCas9 protein fused to the catalytic core of human acetyltransferase p300 and single guide RNA that targets specific genomic loci offers a more flexible approach to enable gene activation via targeted histone acetylation (Hilton et al., 2015). In this study, we have demonstrated the effectiveness of this technique in elevating endogenous *Gad1* expression. More importantly, we showed that elevation of *Gad1* using CRISPR-based epigenome editing in Tau mice not only boosted the diminished inhibitory synaptic transmission, but also mitigated the spatial memory deficits. It underscores the therapeutic potential of targeting GABAergic transmission for restoring neural network homeostasis and cognitive functionality in AD.

Currently FDA-approved AD therapies are either acetylcholinesterase (AChE) inhibitors or amyloid beta (Aβ)-directed antibodies. AChE inhibitors have mild effects on some symptoms without modifying the disease progression (Marucci et al., 2021). Aβ antibodies have inconsistent efficacy in slowing cognitive decline with the potential for serious side effects (Rentz et al., 2024). CRISPR/dCas9-based epigenetic editing has the advantage of enabling the precise manipulation of specific genes endogenously. Our proof-of-concept study suggests that epigenetic editing of key genes that are altered in AD provides a novel treatment avenue.

3.4. Limitations of the therapeutic strategy and alternative approaches

So far there are only a few studies that have successfully used this approach to alter gene expression especially for gene activation in brain (Bohnsack et al., 2022; Savell et al., 2019). One possibility of this limitation is the large size of $dCas9^{p300}$ that prevents it from being packaged into AAV (maximal packaging size: ~4.7 kb). In this study, we found the improvement of synaptic and behavioral phenotypes in Tau mice with PFC injection of $dCas9^{p300}$ and $gRNA^{Gad1}$ lentiviruses. However, the lentivirus expression in brain is restricted to small regions and at low levels, which reduces the effectiveness of gene upregulation with this approach in vivo. Future studies will check whether the deactivated Cas9 could be replaced with smaller versions such as CasΦ (Pausch et al., 2020) to accommodate packaging capacity of AAV.

Another restriction factor for the clinical utility of epigenomic editing is the potential off-targeting issue, which is particularly challenging given our limited understanding of the mechanisms that govern epigenetic regulation of gene expression. The transient effects of epigenomic editing may also be a concern if sustained changes are needed. Nevertheless, with proper spatiotemporal control to minimize off-targeting and enhance functional durability, as well as further optimization to increase targeting specificity, expand targeting ranges, and enhance delivery efficiency, CRISPR-based epigenomic editing will offer a powerful tool for controlling biological function and treating diseases (Goell and Hilton, 2021; Nakamura et al., 2021).

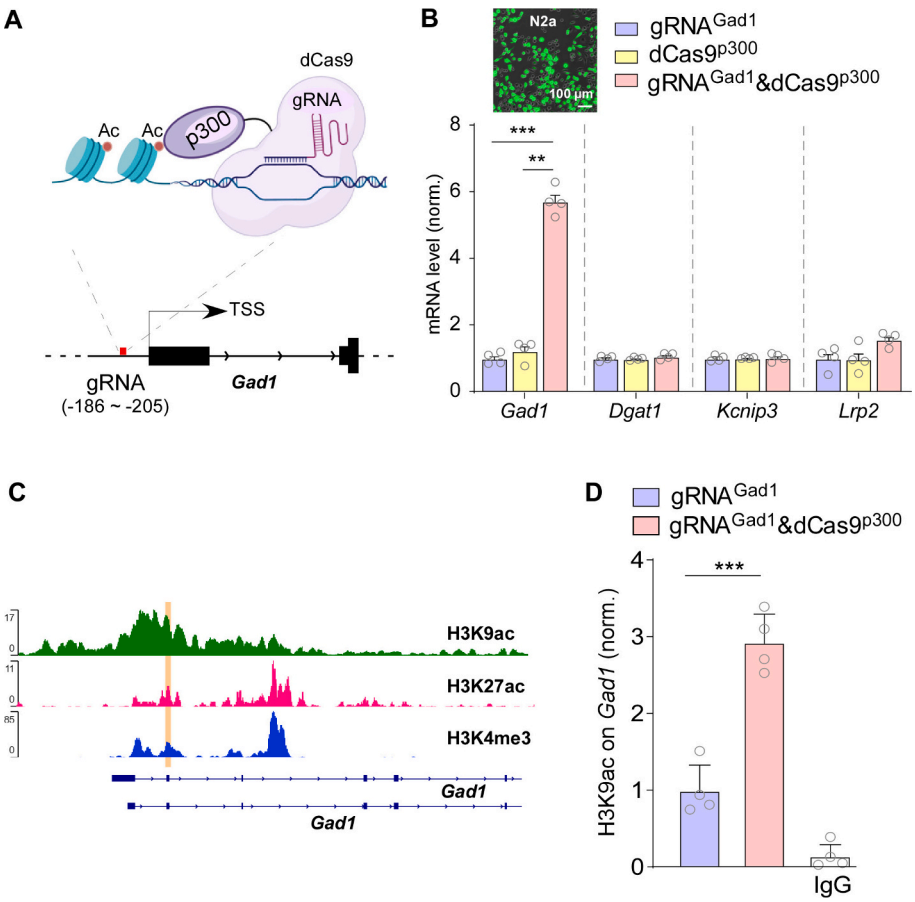

Fig. 4. CRISPR/Cas9 editing of *Gad1* enhances its expression by increasing H3K9ac at its promoter. **A**, Schematic diagram showing epigenetic editing through CRISPR/dCas9 fused with p300 core and gRNA targeting *Gad1* promoter located from 186 to 205 nt upstream of transcription start site (TSS). **B**, Bar graphs showing the mRNA level of *Gad1* and 3 other potential off-target genes (*Dgat1, Kcnip3, Lrp2*) in N2a cells transfected with $gRNA^{Gad1}$&$dCas9^{p300}$ or two controls ($gRNA^{Gad1}$ alone, $dCas9^{p300}$ alone) ($n = 4$/group; $P < 0.001$, $gRNA^{Gad1}$&$dCas9^{p300}$ vs. $gRNA^{Gad1}$, $P < 0.01$, $gRNA^{Gad1}$&$dCas9^{p300}$ vs. $dCas9^{p300}$, one-way ANOVA). Inset: A representative image of N2a cells transfected with $dCas9^{p300}$ and $gRNA^{Gad1}$ (GFP-tagged) plasmids for 48 h. Scale bar: 100 μm. **C**, ChIP-seq landscape showing the occupancy of H3K9ac, H3K27ac, and H3K4me3 at *Gad1* promotor region. The location of primers used in ChIP assays is highlighted with orange. **D**, ChIP assay data showing H3k9ac levels at *Gad1* promotor in N2a cells transfected with $gRNA^{Gad1}$ alone or $gRNA^{Gad1}$&$dCas9^{p300}$ plasmids (n = 4/group, t-test). IgG control is also shown. All data are shown as mean ± SEM. **P < 0.01, ***P < 0.001.

4. Materials and methods

4.1. Animals and human postmortem brain tissue

All experiments were performed with the approval of the State University of New York at Buffalo IACUC Committee. The PS19 mouse line harboring the T34 isoform of microtubule-associated protein tau encoding the human P301S mutation (Yoshiyama et al., 2007) was maintained as we previously described (Cao et al., 2020; Wang et al., 2021; Williams et al., 2023). Both male and female P301S mice (3–6 months old) and age-matched WT littermates were used. There were no sex-dependent effects in our measurements, so data from both males and females were pooled together.

Postmortem human frontal cortex (Brodmann's area 10) from AD patients and control subjects was provided by NeuroBioBank of National Institutes of Health (NIH), as used in our previous studies (Cao et al., 2020; Williams et al., 2023). Information about these individuals was included in **Sup. Table 4**. The average age was 78, and most AD cases were at Braak Stage 5–6. Upon arrival, tissue was stored in a − 80 °C freezer.

4.2. Bioinformatic analysis

AD human microarray dataset (Zhang et al., 2013) and RNAseq datasets from Mayo Clinic and Mount Sinai (Allen et al., 2016; Wang et al., 2018), as well as AD mouse (P301S Tau) RNA-seq dataset (GSE129797) (Wu et al., 2019), were used for bioinformatic analyses. SYNGO [https://www.syngoportal.org/] (Koopmans et al., 2019) was used to examine the enrichment of genes associated with synapses. EnrichR [https://maayanlab.cloud/Enrichr/] (Kuleshov et al., 2016; Xie et al., 2021) was used to identify enriched categories of the differentially expressed genes (DEGs). String database [https://string.db] (Szklarczyk et al., 2021) was used to create protein-protein interaction (PPI) networks. Gene expression changes across AD pseudo-progression in different cell types were obtained from Seattle Alzheimer's Disease Brain Cell Atlas (SEA-AD) [https://sea-ad.shinyapps.io/ad_gene_trajectories/].

4.3. Plasmids construction

Single guide RNA (sgRNA) against mouse *Gad1* promoter (fwd: 5′-caccgCTGGTCGCAAACCCGTGAGC-3′, rev: 5′-aaacGCTCACGGGTTTGCGACCAGc-3′) was designed with filtering tools [https://crispor.gi.ucsc.edu/crispor.py]. To generate the sgRNA plasmid, oligonucleotides were annealed in the following reaction: 10 μM guide sequence oligo, 10 μM reverse complement oligo, T4 ligation buffer (1×), and 5 U of T4 polynucleotide kinase (NEB) with the cycling parameters of 37 °C for 30 min; 95 °C for 5 min and then ramp down to

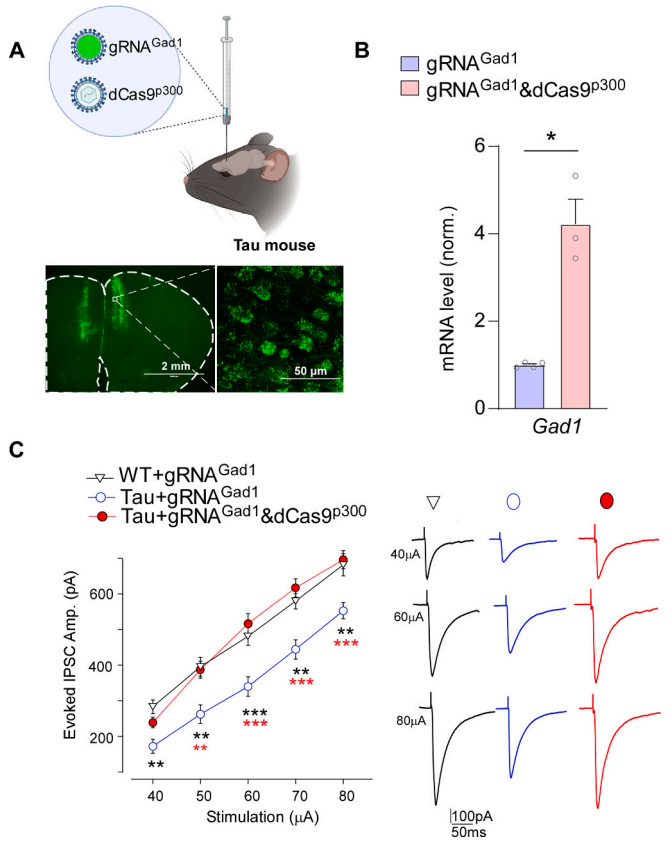

Fig. 5. CRISPR/Cas9 editing of Gad1 elevates gene expression and restores GABAergic synaptic currents in Tau mice. **A**, Images of PFC slices from Tau mice with the stereotaxic injection of gRNA^{Gad1} (GFP-tagged) and dCas9^{p300} lentiviruses. Inset: confocal images of PFC GFP+ cells. **B**, Bar graphs showing the mRNA level of *Gad1* in PFC of mice with stereotaxic injection of gRNA^{Gad1}&dCas9^{p300} lentiviruses or gRNA^{Gad1} alone (gRNA^{Gad1}: n = 4, gRNA^{Gad1}&dCas9^{p300}: n = 3, P = 0.03, t-test). **C**, Input-output curves of evoked GABA$_A$R-IPSC in PFC pyramidal neurons from WT and Tau mice injected with gRNA^{Gad1}&dCas9^{p300} lentiviruses or gRNA^{Gad1} alone (WT + gRNA^{Gad1}: n = 9 cells/3 mice; Tau+gRNA^{Gad1}: n = 10 cells/3 mice; Tau+gRNA^{Gad1}&dCas9^{p300}: n = 13 cells/4 mice. ** P < 0.01; ***P < 0.001, two-way rmANOVA, black: Tau+gRNA^{Gad1} vs. WT + gRNA^{Gad1}; red: Tau+gRNA^{Gad1} vs. Tau+gRNA^{Gad1}&dCas9^{p300}). (For interpretation of the references to colour in this figure legend, the reader is referred to the web version of this article.)

25 °C at 5 °C/min. The annealed oligos were cloned into the sgRNA vectors using Golden Gate Assembly strategy including: 100 ng circular sgRNA vector plasmid (Addgene, #138461), 0.2 μM annealed oligos, 1× T4 DNA ligase buffer (NEB), 20 U of *Bbs*I-v2 restriction enzyme (NEB), and 750 U of T4 DNA ligase (NEB) with the cycling parameters of 20 cycles at 42 °C for 5 min, 20 °C for 5 min, followed by 60 °C incubation for 20 min. The product was transformed into competent *E. coli* cells (Thermo Stbl3 or NEB Stable). Insertion of sgRNA was validated by Sanger sequencing. Plasmid used for expression of dCas9^{p300} was obtained from Addgene (#83889).

4.4. N2a cell culture and transfection

Mouse neuroblastoma (N2a) cells were obtained from ATCC (#CCL-131) and were routinely cultured in Dulbecco's Modified Eagle Medium (DMEM, gibco, # 11995–065) containing 10 % fetal bovine serum (56 °C heated for 30 min, gibco #A5256801), 1 % penicillin/streptomycin (gibco, 10378–016) and maintained in a 5 % CO_2, 95 % air humidified incubator at 37 °C. Cells were passaged every three days.

CRISPR/Cas9 and sgRNA plasmids were transfected into N2a cells using the lipofectamine 3000 transfection reagent (Thermo Scientific,

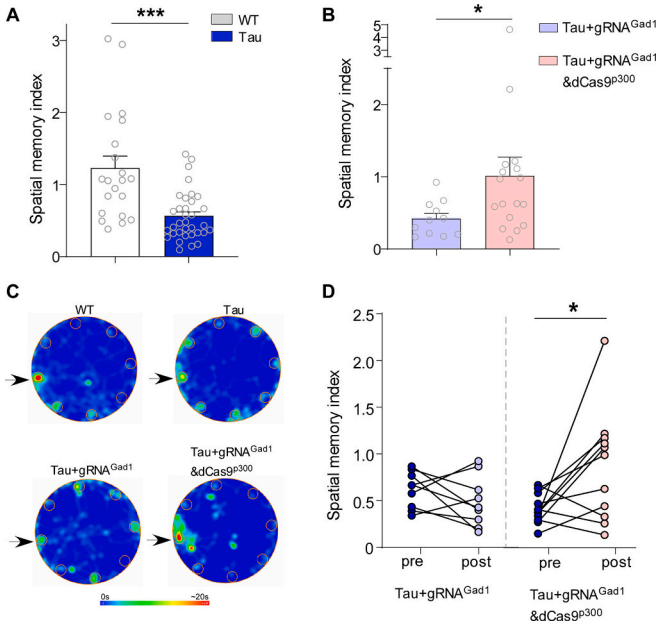

Fig. 6. CRISPR/Cas9 editing of Gad1 ameliorates cognitive deficits in Tau mice. **A**, Bar graphs showing the spatial memory index (T1/T2) in Barnes Maze (BM) tests of WT vs. Tau mice (WT: 1.23 ± 0.17, n = 21, Tau: 0.56 ± 0.06, n = 34, P = 0.0008, t-test). **B**, Bar graphs showing T1/T2 in BM tests of Tau mice with PFC injection of gRNA^{Gad1}&dCas9^{p300} lentiviruses or gRNA^{Gad1} alone (Tau+gRNA^{Gad1}: 0.42 ± 0.07, n = 11, Tau+gRNA^{Gad1}&dCas9^{p300}: 1.01 ± 0.26, n = 17, P = 0.039, t-test). **C**, Representative heatmaps of each group from A and B. **D**, Plot of BM spatial memory index in Tau mice at pre- and post-injection of gRNA^{Gad1}&dCas9^{p300} lentiviruses or gRNA^{Gad1} alone (Tau+gRNA^{Gad1}: 0.61 ± 0.06 (pre); 0.49 ± 0.09 (post), n = 9, P = 0.27; Tau+gRNA^{Gad1}&dCas9^{p300}: 0.43 ± 0.06 (pre); 1.02 ± 0.19 (post), n = 9, P = 0.02, paired t-tests). All data are shown as mean ± SEM. *P < 0.05; ***P < 0.001.

L3000015) according to the manufacturer's manual. Briefly, 70,000 cells were seeded in 12-well plate per well and cultured overnight (~70 % confluency). Before transfection, cells were changed with the fresh medium. For each well, 100 μl opti-MEM Medium, 1 or 2 μg DNA (1 μg sgRNA^{Gad1} plasmid mixed with 1 μg dCad9^{p300} plasmid for dual transfection; 1 μg sgRNA^{Gad1} plasmid alone or 1 μg dCad9^{p300} plasmid alone for single transfection), 2 μl P3000 reagent and 1.5 μl Lipofectamine 3000 reagent were used. The medium containing the transfection solution was replaced with fresh medium after overnight incubation and the transfection efficiency was determined using EVOS Cell Imaging Systems (Thermo Scientific) at 48 h after transfection before immediate harvesting. The transfection efficiency was 60 %–70 %.

4.5. Quantitative real-time PCR

Total RNA was isolated with Trizol reagent (Invitrogen, 15596026). iScriptTM cDNA synthesis Kit (Bio-Rad, 1708891) was used to obtain cDNA from the mRNA. Quantitative real-time PCR was carried out using the CFX Connect Real-Time PCR Detection System and iQ™ SYBR® Green Supermix (Bio-Rad, 1708882). GAPDH was used as the housekeeping gene for quantitation of the expression of target genes. A total reaction mixture of 20 μl was amplified in a 96-well thin-well PCR plate (Bio-Rad, HSP9601) using the following PCR cycling parameters: 95 °C for 3 min followed by 39 cycles of 95 °C for 15 s, 60 °C for 45 s, and followed by melt curve analysis with 55–95 °C, 0.5 °C increment, and 5 s/step. Fold changes in the target genes were calculated as following: ΔCt = Ct(target) – Ct(GAPDH), and Δ(ΔCt) = ΔCt(Tau mice) – mean ΔCt (WT mice), and Fold change = $2^{-\Delta(\Delta Ct)}$. To find out potential off-targets of Gad1 sgRNA, we employed the CRISPR-Cas9 guide RNA design checker tool [https://www.idtdna.com/site/order/designtool/index/

CRISPR_CUSTOM]. Those genes with their promoters having ≤4 nucleotide (nt) mismatches compared to Gad1 sgRNA guide sequence (20-nt) were included as potential off-targets for further examination. All primers used are included in **Sup. Table 5**.

4.6. Western blot

Frontal cortical tissues (50 mg) from human subjects were homogenized with 1 % Sodium Dodecyl Sulfate (SDS) lysis buffer (350 μl) containing protease inhibitor (Thermo Scientific, A32953). The homogenate was boiled for 10 min and followed by centrifugation at 17,000 xg, 4 °C for 15 min. The supernatant was collected and used for quantification with the Pierce™ BCA protein assay kit (Thermo Scientific, 23227).

Protein from each sample (10 or 20 μg) was boiled for 10 min in 4× loading buffer (0.25 M Tris-HCl (pH 6.8), 8 % (*w/v*) SDS, 40 % (*v/v*) Glycerol, 0.02 % (w/v) Bromophenol Blue, 5 % 2-mercaptoethanol) and loaded onto a 10 % SDS-PAGE gel for electrophoresis. Proteins were transferred onto nitrocellulose membrane using the Trans-Blot Turbo Transfer System (Bio-Rad). Membranes were incubated with non-fat milk to block non-specific background, then were incubated with a primary antibody (anti-GAD67, Cell Signaling #41318, 1:1000, or anti-GAPDH, Cell Signaling #5174, 1:2000) at 4 °C overnight. After washing with TBST buffer three times, membranes were blotted with a secondary antibody (anti-mouse 1:2000, GE Lifesciences, NA931, or anti-rabbit 1:2000, GE Lifesciences, NA934) IgG coupled to peroxidase at room temperature for 1 h. After washing, ECL (SuperSignal West-Pico #34577, Thermo Fisher, Waltham, MA, USA) was used to develop membranes. The Integrated Density of each band was measured with ImageJ software.

4.7. Animal surgery

Lenti viral particles ($sgRNA^{Gad1}$: 3 × 10^9 IU/ml; $dCas9^{p300}$: 4 × 10^8 IU/ml) were produced by the viral core center of Emory University. Mice were anesthetized with Ketamine/ xylazine and placed on stereotaxic apparatus (Stoelting, 51730D). Bilateral stereotaxic injection of lentivirus $sgRNA^{Gad1}$ (0.75 μL per hemisphere) or $sgRNA^{Gad1}$&$dCas9^{p300}$ (1:1 mixture, 1.5 μL per hemisphere) into PFC (2.0 mm anterior to bregma; 0.3 mm lateral and 2.0 mm dorsal to ventral) was performed with a Hamilton syringe (gauge 31) at a speed of 0.1 μl/min. After injection, the needle was kept in place for an additional 10 min. All experiments were conducted 2–4 weeks after surgery.

4.8. Electrophysiological recordings

Mice were rapidly decapitated after being anesthetized with isoflurane. Brains were quickly removed and submerged into the ice-cold sucrose solution (in mM: 234 sucrose, 4 $MgSO_4$, 2.5 KCl, 1 NaH_2PO_4, 0.1 $CaCl_2$, 15 HEPES, 11 glucose). Coronal slices (300 μm) were cut on a vibratome (Leica VT1000s), then transferred into oxygenated artificial cerebrospinal fluid (ACSF) (in mM: 130 NaCl, 26 $NaHCO_3$, 3 KCl, 5 $MgCl_2$, 1.25 NaH_2PO_4, 1 $CaCl_2$, 10 Glucose), and kept at 32 °C for 1 h and then at the room temperature (22–24 °C) for 1–4 h. For recordings, the slice was positioned in a perfusion chamber attached to the fixed stage of an upright microscope (Olympus) and submerged in continuously flowing oxygenated ACSF. Whole-cell patch-clamp experiments were performed with a Multiclamp 700 A amplifier and Digidata 1322 A data acquisition system (Molecular Devices). Neurons were visualized with the infrared differential interference contrast video microscopy. Data were acquired using the software Clampex 9.2 (Molecular Device). Recording electrodes were pulled from borosilicate glass capillaries (1.5/0.86 mm OD/ID) with a micropipette puller (Sutter Instrument, P-97). The resistance of patch electrode was ~3 MΩ.

As we previously described (Cao et al., 2020; Qin et al., 2021; Wang et al., 2021; Zheng et al., 2019), whole-cell voltage-clamp recordings were used to measure synaptic currents in medial PFC layer V pyramidal neurons. For $GABA_A$R-IPSC recordings, the internal solution contained (in mM) 100 CsCl, 30 *N*-methyl-D-glucamine, 10 HEPES, 4 NaCl, 1 $MgCl_2$, 5 EGTA, 2 QX-314, 12 phosphocreatine, 5 MgATP, 0.5 Na_2GTP, pH 7.2–7.3, 265–270 mOsm. D-APV (25 μM) and CNQX (20 μM) were added to ACSF. Neurons were held at −70 mV. Evoked IPSC was elicited by a series of current pulses (40–80 μA, delivered at 0.05 Hz) from S48 stimulator (Grass Technologies) via a bipolar stimulating electrode (FHC) that placed ~100 μm apart from the recording neuron. Paired-pulse ratio (PPR) was evoked by two pulses with various intervals (25–200 ms).

4.9. Chromatin immunoprecipitation (CHIP)

ChIP assay was performed as we previously described (Qin et al., 2021; Zheng et al., 2019). After 48 h of transfection, N2a cells were collected in 250 μl ice cold bouncing buffer (10 mM Tris-HCl, pH 7.5, 4 mM $MgCl_2$, 1 mM $CaCl_2$) and homogenized with 1 ml 26-gauge syringe for 6 times. The homogenized sample was incubated with micrococcal nuclease (5 U/ml, Sigma, N5386) for 7 min at 37 °C and terminated by adding EDTA (10 mM, Invitrogen, 15575–038). The samples were incubated with 0.4 ml hypotonic lysis buffer (10 mM Tris-HCl, pH 7.4, 0.2 mM EDTA, pH 8.0, 50 mM NaCl, 0.1 mM benzamidine, 0.1 mM PMSF, 50 % Glycerol, 0.1 mM PMSF and 1.5 mM DTT) with protease inhibitor on ice for 1 h with brief vortex every 10 min. The supernatant was collected after centrifugation at 3000 xg for 5 min at 4 °C. After adding 10 × incubation buffer (50 mM EDTA, 200 mM Tris-HCl, 500 mM NaCl), 10 % supernatant was saved as input control. To reduce nonspecific background, the supernatant was pre-cleared with 60 μl salmon sperm DNA/protein A agarose-50 % slurry (Millipore, 16–157) for 1 h at 4 °C with agitation. The pre-cleared supernatant was incubated with antibodies against H3K9ac (Cell Signaling, 9649) or Rabbit IgG (Sigma Aldrich, 12–370) (4 μg per reaction) overnight at 4 °C under constant rotation, followed by incubation with 60 μl Salmon Sperm DNA/Protein A agarose 50 % Slurry for 2 h at 4 °C. After washing with Low salt wash buffer, High salt wash buffer, LiCl wash buffer and TE buffer (twice), bound complex was eluted twice from the beads by incubating with the elution buffer (1 % SDS, 0.1 M $NaHCO_3$) at room temperature. EDTA (0.5 M, 8 μl), NaCl (5 M, 16 μl), Tris-HCl (10 mM, 16 μl, pH 7.4), RNaseA (10 mg/ml, 0.4 ul) and proteinase K (20 mg/ml, 0.8 μl, Thermo Fisher, EO0491) were used to combine eluates and inputs and incubated for 1 h at 60 °C. Immunoprecipitated DNA and input DNA were purified by QIAquick PCR purification Kit (Qiagen, 28104). Buffer EB (30 μl, Qiagen, 19086) was used for DNA dissolution. Oligos used in ChIP-qPCR were designed against Gad1 promoter region (Forward: 5'-TTAGCTGTGAGCCTCACTCG, Reverse: 5'-ACCGAAGTCTCGGAGACAGAA). Quantification of ChIP signals was calculated as % input.

4.10. Behavioral testing

Barnes maze (BM) test was carried out as we previously described (Cao et al., 2020; Wang et al., 2021; Williams et al., 2023; Zheng et al., 2019). In brief, mice were transferred to dim lighted testing room for one-hour habituation. Then the mouse was placed on a round platform with eight equally spaced holes at the edge, one of which was attached with an escape box at the bottom (correct hole). Signs of different colors and shapes on the surrounding walls were used as visual cues. A strong light was shed on the platform as a stimulation to increase the motivation of escaping. Each mouse had 3 learning phases (5-min interval) to find the correct hole based on the visual cues and enter the escape box. Then, the mouse had a 15-min rest in a holding cage. In the testing phase (5-min), the escape box was removed, the mouse was put back on the platform, and the time spent on the correct hole (T1) and the other seven incorrect holes (T2) were recorded. Spatial memory index was calculated as T1/T2.

4.11. Statistical analysis

Data were analyzed with GraphPad Prism 7 (GraphPad), Clampfit (Molecular Devices, Sunnyvale, CA), and Mini analysis (Synaptosoft, NJ). All values were means ± SEM. Differences between two groups were assessed with unpaired two-tailed Student's *t*-test unless otherwise stated. Differences between more than two groups were assessed with one-way or two-way ANOVA, followed by post hoc Bonferroni tests for multiple comparisons.

CRediT authorship contribution statement

Lei Wan: Writing – original draft, Investigation, Formal analysis, Data curation, Conceptualization. **Ping Zhong:** Investigation, Formal analysis, Data curation. **Pei Li:** Formal analysis, Data curation. **Yong Ren:** Formal analysis, Data curation. **Wei Wang:** Formal analysis, Data curation. **Mingjun Yu:** Formal analysis, Data curation. **Henry Y. Feng:** Formal analysis, Data curation. **Zhen Yan:** Writing – review & editing, Supervision, Funding acquisition, Conceptualization.

Declaration of competing interest

The authors report no competing financial or other interests.

Acknowledgements

We thank NIH NeuroBioBank for providing postmortem brain tissues from AD patients and control subjects. This work was supported by grants from the National Institutes of Health AG064656 to Z.Y. and AG067597 to Z.Y.

Appendix A. Supplementary data

Supplementary data to this article can be found online at https://doi.org/10.1016/j.nbd.2025.106826.

Data availability

Data will be made available on request.

References

Allen, M., Carrasquillo, M.M., Funk, C., Heavner, B.D., Zou, F., et al., 2016. Human whole genome genotype and transcriptome data for Alzheimer's and other neurodegenerative diseases. Sci. Data 3, 160089.
Bohnsack, J.P., Zhang, H., Wandling, G.M., He, D., Kyzar, E.J., et al., 2022. Targeted epigenomic editing ameliorates adult anxiety and excessive drinking after adolescent alcohol exposure. Sci. Adv. 8, eabn2748.
Brose, N., O'Connor, V., Skehel, P., 2010. Synaptopathy: dysfunction of synaptic function? Biochem. Soc. Trans. 38, 443–444.
Bustos, F.J., Ampuero, E., Jury, N., Aguilar, R., Falahi, F., et al., 2017. Epigenetic editing of the Dlg4/PSD95 gene improves cognition in aged and Alzheimer's disease mice. Brain 140, 3252–3268.
Cao, Q., Wang, W., Williams, J.B., Yang, F., Wang, Z.J., Yan, Z., 2020. Targeting histone K4 trimethylation for treatment of cognitive and synaptic deficits in mouse models of Alzheimer's disease. Sci. Adv. 6.
Cao, Q., Kumar, M., Frazier, A., Williams, J.B., Zhao, S., Yan, Z., 2023. Longitudinal characterization of behavioral, morphological and transcriptomic changes in a tauopathy mouse model. Aging (Albany NY) 15, 11697–11719.
Cappelluti, M.A., Mollica Poeta, V., Valsoni, S., Quarato, P., Merlin, S., et al., 2024. Durable and efficient gene silencing in vivo by hit-and-run epigenome editing. Nature 627, 416–423.
Carello-Collar, G., Bellaver, B., Ferreira, P.C.L., Ferrari-Souza, J.P., Ramos, V.G., et al., 2023. The GABAergic system in Alzheimer's disease: a systematic review with meta-analysis. Mol. Psychiatry 28, 5025–5036.
De Strooper, B., Karran, E., 2016. The cellular phase of Alzheimer's disease. Cell 164, 603–615.
Froemke, R.C., 2015. Plasticity of cortical excitatory-inhibitory balance. Annu. Rev. Neurosci. 38, 195–219.
Gabitto, M.I., Travaglini, K.J., Rachleff, V.M., Kaplan, E.S., Long, B., et al., 2024. Integrated multimodal cell atlas of Alzheimer's disease. Nature Neuroscience 27, 2366–2383.
Garcia-Cabrero, A.M., Guerrero-Lopez, R., Giraldez, B.G., Llorens-Martin, M., Avila, J., et al., 2013. Hyperexcitability and epileptic seizures in a model of frontotemporal dementia. Neurobiol. Dis. 58, 200–208.
Ghatak, S., Talantova, M., McKercher, S.R., Lipton, S.A., 2021. Novel therapeutic approach for excitatory/inhibitory imbalance in neurodevelopmental and neurodegenerative diseases. Annu. Rev. Pharmacol. Toxicol. 61, 701–721.
Goell, J.H., Hilton, I.B., 2021. CRISPR/Cas-based epigenome editing: advances, applications, and clinical utility. Trends Biotechnol. 39, 678–691.
Govindpani, K., Turner, C., Waldvogel, H.J., Faull, R.L.M., Kwakowsky, A., 2020. Impaired expression of GABA signaling components in the Alzheimer's disease middle temporal gyrus. Int. J. Mol. Sci. 21.
Harris, S.S., Wolf, F., De Strooper, B., Busche, M.A., 2020. Tipping the scales: peptide-dependent dysregulation of neural circuit dynamics in Alzheimer's disease. Neuron 107, 417–435.
Hill, M.A., Gammie, S.C., 2022. Alzheimer's disease large-scale gene expression portrait identifies exercise as the top theoretical treatment. Sci. Rep. 12, 17189.
Hilton, I.B., D'Ippolito, A.M., Vockley, C.M., Thakore, P.I., Crawford, G.E., et al., 2015. Epigenome editing by a CRISPR-Cas9-based acetyltransferase activates genes from promoters and enhancers. Nat. Biotechnol. 33, 510–517.
Huber, N., Korhonen, S., Hoffmann, D., Leskela, S., Rostalski, H., et al., 2022. Deficient neurotransmitter systems and synaptic function in frontotemporal lobar degeneration-insights into disease mechanisms and current therapeutic approaches. Mol. Psychiatry 27, 1300–1309.
Kazim, S.F., Seo, J.H., Bianchi, R., Larson, C.S., Sharma, A., et al., 2021. Neuronal network excitability in Alzheimer's disease: the puzzle of similar versus divergent roles of amyloid beta and tau. eNeuro 8.
Kiernan, M.C., Vucic, S., Cheah, B.C., Turner, M.R., Eisen, A., et al., 2011. Amyotrophic lateral sclerosis. Lancet 377, 942–955.
Knopman, D.S., Amieva, H., Petersen, R.C., Chetelat, G., Holtzman, D.M., et al., 2021. Alzheimer disease. Nat. Rev. Dis. Primers 7, 33.
Koopmans, F., van Nierop, P., Andres-Alonso, M., Byrnes, A., Cijsouw, T., et al., 2019. SynGO: an evidence-based, expert-curated Knowledge Base for the synapse. Neuron 103 (217–34), e4.
Kuleshov, M.V., Jones, M.R., Rouillard, A.D., Fernandez, N.F., Duan, Q., et al., 2016. Enrichr: a comprehensive gene set enrichment analysis web server 2016 update. Nucleic Acids Res. 44, W90–W97.
Lauterborn, J.C., Scaduto, P., Cox, C.D., Schulmann, A., Lynch, G., et al., 2021. Increased excitatory to inhibitory synaptic ratio in parietal cortex samples from individuals with Alzheimer's disease. Nat. Commun. 12, 2603.
Li, J.Y., Plomann, M., Brundin, P., 2003. Huntington's disease: a synaptopathy? Trends Mol. Med. 9, 414–420.
Li, K., Liu, Y., Cao, H., Zhang, Y., Gu, Z., et al., 2020. Interrogation of enhancer function by enhancer-targeting CRISPR epigenetic editing. Nat. Commun. 11, 485.
Liu, X.S., Jaenisch, R., 2019. Editing the epigenome to tackle brain disorders. Trends Neurosci. 42, 861–870.
Long, J.M., Holtzman, D.M., 2019. Alzheimer disease: an update on pathobiology and treatment strategies. Cell 179, 312–339.
Maeda, S., Djukic, B., Taneja, P., Yu, G.Q., Lo, I., et al., 2016. Expression of A152T human tau causes age-dependent neuronal dysfunction and loss in transgenic mice. EMBO Rep. 17, 530–551.
Mandolesi, G., Gentile, A., Musella, A., Fresegna, D., De Vito, F., et al., 2015. Synaptopathy connects inflammation and neurodegeneration in multiple sclerosis. Nat. Rev. Neurol. 11, 711–724.
Marinkovic, P., Blumenstock, S., Goltstein, P.M., Korzhova, V., Peters, F., et al., 2019. In vivo imaging reveals reduced activity of neuronal circuits in a mouse tauopathy model. Brain 142, 1051–1062.
Marucci, G., Buccioni, M., Ben, D.D., Lambertucci, C., Volpini, R., Amenta, F., 2021. Efficacy of acetylcholinesterase inhibitors in Alzheimer's disease. Neuropharmacology 190, 108352.
Mathys, H., Peng, Z., Boix, C.A., Victor, M.B., Leary, N., et al., 2023. Single-cell atlas reveals correlates of high cognitive function, dementia, and resilience to Alzheimer's disease pathology. Cell 186 (4365–85), e27.
Mori, H., Yoshino, Y., Iga, J.I., Ochi, S., Funahashi, Y., et al., 2023. Aberrant expression of GABA-related genes in the Hippocampus of 3xTg-AD model mice from the early to end stages of Alzheimer's disease. J. Alzheimers Dis. 94, 177–188.
Mucke, L., Selkoe, D.J., 2012. Neurotoxicity of amyloid beta-protein: synaptic and network dysfunction. Cold Spring Harb. Perspect. Med. 2, a006338.
Nakamura, M., Gao, Y., Dominguez, A.A., Qi, L.S., 2021. CRISPR technologies for precise epigenome editing. Nat. Cell Biol. 23, 11–22.
Neumann, E.N., Bertozzi, T.M., Wu, E., Serack, F., Harvey, J.W., et al., 2024. Brainwide silencing of prion protein by AAV-mediated delivery of an engineered compact epigenetic editor. Science 384, ado7082.
Okur, Z., Schlauri, N., Bitsikas, V., Panopoulou, M., Ortiz, R., et al., 2024. Control of neuronal excitation-inhibition balance by BMP-SMAD1 signalling. Nature 629, 402–409.
Palop, J.J., Mucke, L., 2016. Network abnormalities and interneuron dysfunction in Alzheimer disease. Nat. Rev. Neurosci. 17, 777–792.
Pasinelli, P., Brown, R.H., 2006. Molecular biology of amyotrophic lateral sclerosis: insights from genetics. Nat. Rev. Neurosci. 7, 710–723.
Pausch, P., Al-Shayeb, B., Bisom-Rapp, E., Tsuchida, C.A., Li, Z., et al., 2020. CRISPR-CasPhi from huge phages is a hypercompact genome editor. Science 369, 333–337.
Pulecio, J., Verma, N., Mejía-Ramírez, E., Huangfu, D., Raya, A., 2017. CRISPR/Cas9-based engineering of the epigenome. Cell Stem Cell 21, 431–447.
Qin, L., Williams, J.B., Tan, T., Liu, T., Cao, Q., et al., 2021. Deficiency of autism risk factor ASH1L in prefrontal cortex induces epigenetic aberrations and seizures. Nat. Commun. 12, 6589.

Rentz, D.M., Aisen, P.S., Atri, A., Hitchcock, J., Irizarry, M., et al., 2024. Benefits and risks of FDA-approved amyloid-targeting antibodies for treatment of early Alzheimer's disease: navigating clinician-patient engagement. Alzheimers Dement. 20, 8162–8171.
Savell, K.E., Bach, S.V., Zipperly, M.E., Revanna, J.S., Goska, N.A., et al., 2019. A neuron-optimized CRISPR/dCas9 activation system for robust and specific gene regulation. eNeuro 6.
Selkoe, D.J., 2002. Alzheimer's disease is a synaptic failure. Science 298, 789–791.
Szklarczyk, D., Gable, A.L., Nastou, K.C., Lyon, D., Kirsch, R., et al., 2021. The STRING database in 2021: customizable protein-protein networks, and functional characterization of user-uploaded gene/measurement sets. Nucleic Acids Res. 49, D605–D612.
Thakore, P.I., Black, J.B., Hilton, I.B., Gersbach, C.A., 2016. Editing the epigenome: technologies for programmable transcription and epigenetic modulation. Nat. Methods 13, 127–137.
Van Erum, J., Valkenburg, F., Van Dam, D., Deyn, De, 2020. Pentylenetetrazole-induced seizure susceptibility in the Tau58/4 transgenic mouse model of Tauopathy. Neuroscience 425, 112–122.
Verret, L., Mann, E.O., Hang, G.B., Barth, A.M., Cobos, I., et al., 2012. Inhibitory interneuron deficit links altered network activity and cognitive dysfunction in Alzheimer model. Cell 149, 708–721.
Vossel, K.A., Tartaglia, M.C., Nygaard, H.B., Zeman, A.Z., Miller, B.L., 2017. Epileptic activity in Alzheimer's disease: causes and clinical relevance. Lancet Neurol. 16, 311–322.
Wang, M., Beckmann, N.D., Roussos, P., Wang, E., Zhou, X., et al., 2018. The Mount Sinai cohort of large-scale genomic, transcriptomic and proteomic data in Alzheimer's disease. Sci. Data 5, 180185.
Wang, W., Cao, Q., Tan, T., Yang, F., Williams, J.B., Yan, Z., 2021. Epigenetic treatment of behavioral and physiological deficits in a tauopathy mouse model. Aging Cell 20, e13456.
Williams, J.B., Cao, Q., Yan, Z., 2021. Transcriptomic analysis of human brains with Alzheimer's disease reveals the altered expression of synaptic genes linked to cognitive deficits. Brain Commun. 3, fcab123.
Williams, J.B., Cao, Q., Wang, W., Lee, Y.H., Qin, L., et al., 2023. Inhibition of histone methyltransferase Smyd3 rescues NMDAR and cognitive deficits in a tauopathy mouse model. Nat. Commun. 14, 91.
Wilson 3rd, D.M., Cookson, M.R., Van Den Bosch, L., Zetterberg, H., Holtzman, D.M., Dewachter, I., 2023. Hallmarks of neurodegenerative diseases. Cell 186, 693–714.
Wu, T., Dejanovic, B., Gandham, V.D., Gogineni, A., Edmonds, R., et al., 2019. Complement C3 is activated in human AD brain and is required for neurodegeneration in mouse models of amyloidosis and Tauopathy. Cell Rep. 28, 2111-23.e6.
Xie, Z., Bailey, A., Kuleshov, M.V., Clarke, D.J.B., Evangelista, J.E., et al., 2021. Gene set knowledge discovery with Enrichr. Curr. Protoc. 1, e90.
Yoshiyama, Y., Higuchi, M., Zhang, B., Huang, S.M., Iwata, N., et al., 2007. Synapse loss and microglial activation precede tangles in a P301S tauopathy mouse model. Neuron 53, 337–351.
Zhang, B., Gaiteri, C., Bodea, L.G., Wang, Z., McElwee, J., et al., 2013. Integrated systems approach identifies genetic nodes and networks in late-onset Alzheimer's disease. Cell 153, 707–720.
Zheng, Y., Liu, A., Wang, Z.J., Cao, Q., Wang, W., et al., 2019. Inhibition of EHMT1/2 rescues synaptic and cognitive functions for Alzheimer's disease. Brain 142, 787–807.
Zhong, M.Z., Peng, T., Duarte, M.L., Wang, M., Cai, D., 2024. Updates on mouse models of Alzheimer's disease. Mol. Neurodegener. 19, 23.